

EVIDENCE OF THICK OBSCURING MATTER REVEALED IN THE X-RAY SPECTRUM OF THE $Z=4.28$ QUASAR RX J1028.6-0844

W. YUAN¹, M. MATSUOKA¹, T. WANG², S. UENO¹, H. KUBO³, T. MIHARA⁴
Draft version October 28, 2018

ABSTRACT

We report the discovery of an unambiguous, substantial low-energy cutoff in the broad band X-ray spectrum of the radio quasar RX J1028.6-0844 at a redshift of 4.276 obtained with the ASCA satellite, which we preferably explained as indication of excess X-ray absorption. The equivalent hydrogen column density of the absorbing matter, depending on the redshift and metallicity, ranges from $2.5 \times 10^{21} \text{ cm}^{-2}$ for local absorption up to $2.1 \times 10^{23} \text{ cm}^{-2}$ (solar metallicity) or $1.6 \times 10^{24} \text{ cm}^{-2}$ (10% solar metallicity) for absorption at the quasar redshift. Such a value is among the largest found for high-redshift radio quasars. The absorption, if interpreted as being produced close to the quasar, may indicate the presence of a remarkably large amount of obscuring matter in the quasar environment in the early universe. Implications of the result for the possible origins of the absorbing matter are discussed, concerning especially galactic intervening matter, cool intracluster gas, and ambient medium around the quasar jet. The quasar itself has an enormous apparent luminosity of at least about $2.6 \times 10^{47} \text{ erg s}^{-1}$ ($H_0 = 50 \text{ km s}^{-1} \text{ Mpc}^{-1}$, $q_0 = 0.5$) and a power law photon index of $1.67^{(+0.07, -0.04)}$ in the 2–50 keV band in the source rest frame.

Subject headings: X-rays: ISM – X-rays: galaxies – quasars: individual: RX J1028.6-0844

1. INTRODUCTION

Photoelectric absorption in the soft X-ray spectra of quasars provides unique probes of circum-source matter and quasar evolution. There is growing evidence that radio-loud quasars at high redshifts ($z > 2$) are commonly obscured by opaque matter—the X-ray spectra flatten toward low energies and this is attributed to absorption of the soft X-ray photons in excess of that due to Galactic interstellar medium, known as the excess absorption (Wilkes et al. 1992; Elvis et al. 1994; Serlemitsos et al. 1994; Siebert et al. 1996; Cappi et al. 1997; Reeves et al. 1997; Fiore et al. 1998). It is not known what cause such absorption, nor where they occur. Both, cosmologically intervening and quasar-associated materials are proposed as absorber candidates; and the latter is favored by statistical arguments (Bechtold et al. 1994; O’Flaherty and Jakobsen 1997; Fiore et al. 1998; Yuan and Brinkmann 1999) for high- z radio-quiet quasars showing no excess absorption, and by tentative indications for variability of the absorption (e.g. Schartel et al. 1997, Cappi et al. 1997). This picture has been established based mainly on observations of quasars in the redshift range of 2–4. The highest redshifts up to which the excess absorption was reported in these observations are of PKS 2126-158 at $z = 3.3$ (Elvis et al. 1994) and of S5 0014+81 at $z = 3.4$ (Cappi et al. 1997), and probably of Q1745+624 at $z = 3.9$ (Kubo et al. 1997).

At even higher redshifts ($z > 4$), only two quasars, both radio-loud, were observed with fair broad band X-ray spectroscopy, 1508+5714 at $z=4.3$ (Moran and Helfand 1997) and GB 1428+4217 at $z=4.7$ (Fabian et al. 1998). While the ASCA spectra of both objects do not require excess absorption, GB 1428+4217 was recently reported to have excess absorption with a ROSAT PSPC observation (a hydrogen column

density of $1.52(\pm 0.28) \times 10^{22} \text{ cm}^{-2}$, assuming the absorber associated with the quasar; Boller et al. 2000). Another interesting and probably related aspect is that both objects show blazar properties, i.e. radio and X-ray emission dominated by relativistically beamed components from the jets. Though two objects are too few for any statistical inference, it is intriguing to wonder whether this behavior is typical at very high redshifts or merely selection effects.

In this paper, we report an ASCA observation of the $z > 4$ quasar RX J1028.6-0844, as part of our X-ray high- z quasar program (Matsuoka et al. 1999). The quasar shows an unambiguous, strong low-energy cutoff in its X-ray spectrum. The X-ray source RX J1028.6-0844 was discovered in the ROSAT All-sky Survey (RASS) and identified with a quasar at $z = 4.276$ by Zickgraf et al. (1997). Its X-ray colors in the ROSAT energy band indicated an extremely hard spectrum, thus, strong X-ray absorption if the ‘intrinsic’ spectrum is of typical radio-loud quasars (Zickgraf et al. 1997). The object is also associated with a radio source, PKS B1026-084 (Otrupcek & Wright 1991), which has a flux density of 220 mJy at 5 GHz and a flat radio spectrum ($\alpha = 0.3$, $S \propto \nu^{-\alpha}$); hence it is a flat-spectrum radio-loud quasar (FSRQ), and has an intense 5 GHz radio luminosity⁵ $\nu L_\nu = 5 \times 10^{44} \text{ erg s}^{-1}$. We present the observation and data reduction in Sect. 2, and spectral and temporal analyses in Sect. 3 and 4, respectively. In Sect. 5 the implications for the origins of the excess absorption are discussed. A summary of the main results is given in Sect. 6. Errors quoted are of the 68% confidence level (c.l.) throughout the paper unless mentioned otherwise.

2. OBSERVATION AND DATA REDUCTION

¹Space Astrophysics group, National Space Development Agency of Japan (NASDA), Tsukuba Space Center, 2-1-1 Sengen, Tsukuba, Ibaraki 305, Japan Email (YW): ywm@oasis.tksk.nasda.go.jp

²Center for Astrophysics, University of Science and Technology of China, Anhui, 230026, China

³Department of Physics, Tokyo Institute of Technology, 2-12-1, Ookayama, Meguro, Tokyo, 152-8551, Japan

⁴The Institute of Physical and Chemical Research (RIKEN), 2-1, Hirosawa, Wako, Saitama, 351-0198, Japan

⁵ $H_0 = 50 \text{ km s}^{-1} \text{ Mpc}^{-1}$ and $q_0 = 0.5$ are assumed throughout the paper.

RXJ1028.6-0844 was observed with the ASCA satellite (Tanaka et al. 1994) on Nov. 25, 1999 and the duration lasted 67 hours. The Solid-state Imaging Spectrometers (SIS) were operated in the 1-CCD faint mode and the Gas Imaging Spectrometers (GIS) in pulse height mode. For SIS the ‘bright 2’ mode data (grade 0, 2, 3, 4) were used, which were converted from the original faint mode data. Corrections for the dark frame error and the echo effect were applied. The data reduction was performed in the standard way by using the FTOOLS (v.4.2) utilities. Hot and flickering pixels were removed from the SIS data. To improve the reliability of the results, we chose conservative data screening criteria, which are listed in Table 1.

The source counts were extracted from circular regions of 3.5 and 5 arcmin radii for SIS and GIS, respectively. The backgrounds were determined in two ways and compared with each other: from the blank-sky observations using the same region of the detector, and from source-free regions in the field of view of the same observation (local). For the latter, for each of the GIS detectors two local off-source regions were used to extract background events, which were chosen so as to have the same radii and off-axis angles as the source region; for SIS, the background events were extracted from the whole CCD chip with a circular region of 5 arcmin radius around the source excluded. In addition to closely matching the screening criteria, the local backgrounds have the advantages over the blank-sky backgrounds regarding the uncorrected decreasing of the low-energy efficiency for SIS and the variability of the internal background for GIS. This is especially true considering the long time span between the blank-sky and the current observations. We thus mainly used the local backgrounds to derive results and used the blank-sky backgrounds for comparisons. The resulting effective exposures and extracted source counts are given in Table 1.

Since the two GIS have identical response matrices and the two source spectra agree well with each other, we combined them into one single GIS spectrum⁶. All the spectra were rebinned to have at least 30 counts in each energy bin. We used the most updated releases of the response matrices available so far (V4.0 GIS RMF `gis2(3)v4_0.rmf`, V1.1 SIS RMF and the calibration file `siph2pi_110397.fits`) in spectral fit.

3. SPECTRAL ANALYSIS

It is known that the responses of the two SIS suffer from calibration uncertainties, which are the most problematic at around 0.6 keV (ASCA Guest Observer Facility web page). To minimize the possible systematic error introduced in the results, we ignored the SIS data below 0.7 keV in spectral fit, but compared them with the fitted models. The energy ranges used for spectral fits are 0.7–9.5 keV for both SIS and GIS. We first fit the spectra with a simple power law model modified by photoelectric absorption assuming an absorber in the observer frame (local absorption, Sect. 3.1) and at a redshift (redshifted absorption, Sect. 3.2), respectively, in addition to the Galactic absorption. Then we test other spectral models for the continuum in Sect. 3.3. We consider the impact of the excluded low-energy data on the obtained results in Sect. 3.4.

3.1. Power law with local absorption model

The Galactic column density in the source direction is $N_{\text{H}}^{\text{Gal}} = 4.59 \times 10^{20} \text{ cm}^{-2}$ (Dickey & Lockman 1990). A fit with a sin-

gle power law model absorbed by ‘cold’ gas (model *wabs*⁷ in *XSPEC* v.10) with the column density fixed at $N_{\text{H}}^{\text{Gal}}$ gave a flat photon index $\Gamma = 1.34 \pm 0.03$ (joint fit of the SIS0, SIS1, and GIS spectra, see Table 2 for the fitted parameters). Though the model is statistically acceptable, the data below 1 keV fall systematically below the model. The deviations are more pronounced as shown in Fig. 1, in which the above model was fitted to the spectra in the restricted 2.5–9.5 keV band only (13–50 keV in the quasar frame) and extrapolated down to 0.5 keV. Such a low-energy cutoff cannot be explained by the known calibration uncertainty for SIS. This is because, firstly, the GIS spectra, though being less sensitive in the low energy range, show the same effect with similar amounts of deviations as the SIS spectra; secondly, the loss of the SIS efficiencies is quantified as up to about 20–40% at 0.6 keV (ASCA Guest Observer Facility web page), while in this case the deviations of the data from the model are about a factor of two on average, for both SIS and GIS.

Setting the absorption column density N_{H} as a free parameter improved the fits significantly, and yielded large N_{H} for both SIS and GIS. The χ^2 value was reduced by $\Delta\chi^2 = 6, 18,$ and 34 for fitting the GIS, SIS0+SIS1, and the joint GIS+SIS spectra, respectively. Thus, the addition of the excess absorption term is significant at $> 99.99\%$ c.l. For the joint GIS+SIS fit this gave $N_{\text{H}} = 3.0^{(+0.5)}_{(-0.4)} \times 10^{21} \text{ cm}^{-2}$, and a photon index $\Gamma = 1.67^{(+0.07)}_{(-0.04)}$, which is typical of FSRQ in the ~ 1 –10(20) keV band at low and medium redshifts (e.g. Siebert et al. 1996; Lawson and Turner 1997; Reeves et al. 1997; Cappi et al. 1997; Brinkmann et al. 1997). The residuals of the fit are shown in Fig. 2. The SIS 0.5–0.7 keV data, which were excluded from the spectral fitting, are also plotted; it is shown that the extrapolation of the model does not under-predict the count rates in this band (though the real count rates could be somewhat higher because of the loss of the SIS efficiencies). Fig. 3 shows the confidence contours for two interesting parameters for the fitted N_{H} and Γ (marked by $z = 0$). Absorption of the quasar X-rays in excess of that due to the Galactic column density is evident. Using the background spectra derived from the blank-sky observations gave consistent results.

Due to the increasing degradation of the response, the calibration for both SIS is uncertain below ~ 1 keV; this effect reportedly results in deficits of the observed counts at low energies and, effectively, apparent ‘excess absorption’. From the most recent quantification of this problem (Yaqoob et al. 2000), the apparent excess N_{H} at the time of the observation was estimated as (using the 0.5–10 keV data) $\Delta N_{\text{H}} \sim 0.7 \times 10^{21} \text{ cm}^{-2}$ for SIS0 and about $1.0 \times 10^{21} \text{ cm}^{-2}$ for SIS1. Fitting the *whole* 0.5–10 keV SIS spectra yielded $N_{\text{H}} = 2.9^{(+0.7)}_{(-0.5)} \times 10^{21} \text{ cm}^{-2}$ ($\Gamma = 1.62$) for SIS0 and $4.5^{(+1.0)}_{(-0.7)} \times 10^{21} \text{ cm}^{-2}$ ($\Gamma = 1.74$) for SIS1; the resulting excess absorption column densities are significantly larger than the estimated systematic uncertainty. Thus, the observed low-energy cutoff is a true feature of the source spectrum, not an artifact due to the calibration problem. Very roughly, we estimated the ‘true’ absorption column density by subtracting the systematic excess ΔN_{H} from the fitted value, as $N_{\text{H}} - \Delta N_{\text{H}}$. We found that, for both SIS, the remaining column densities are very close to the fitted N_{H} values by using the 0.7–10 keV spectra, for which the calibration uncertainty is thought to have less effect. Independently, the GIS spectrum gave a $N_{\text{H}} = 3.0^{(+1.2)}_{(-1.0)} \times 10^{21} \text{ cm}^{-2}$ in good agreement with that fitted using the

⁶The counting errors in each bin were assigned as pure Poissonian errors of the summed counts.

⁷For which the photoelectric absorption cross sections from Morrison and McCammon (1983) are used.

0.7–10 keV SIS spectra (see Table 2), suggesting that the SIS calibration systematic uncertainties are small and negligible in the 0.7–10 keV band in comparison to the statistical uncertainties. We therefore regard the spectral parameters derived by using the 0.7–10 keV SIS spectra, as performed throughout this work, as being little affected by the calibration uncertainties, and ignore this effect in the following analyses.

For the power law with Galactic absorption model, the absorption corrected 2–10 keV flux is $1.2 \cdot 10^{-12} \text{ erg s}^{-1} \text{ cm}^{-2}$, corresponding to a luminosity of $6.2 \cdot 10^{46}$ ($2.4 \cdot 10^{47}$) erg s^{-1} in the 2–10 (2–50) keV band in the quasar rest frame. For the free absorption model, the luminosity corrected for the *total* (Galactic + excess) absorption is $9.8 \cdot 10^{46}$ ($2.6 \cdot 10^{47}$) erg s^{-1} in the 2–10 (2–50) keV band. These values were obtained using the GIS data, which are slightly higher than the SIS measurements by less than 10%. No iron K emission line was detected; the upper limit of the equivalent width for a narrow ($\sigma = 0.01 \text{ keV}$) line at 6.4 keV is 195 eV at the 90% c.l. in the source rest frame. We found no iron K-shell absorption edge feature for local absorption, setting a 90% upper limit on the optical depth as $\tau < 0.79$ at 7.1 keV.

3.2. Power law with redshifted absorption

3.2.1. Absorption at the quasar redshift

Assuming the absorber is associated with the quasar, we fitted the spectra with models of a power law modified by absorption occurring at $z = 4.276$, and further by the (fixed) Galactic absorption. For ‘cold’ absorption models this results in the same χ^2 with, but a larger excess absorption column density $N_{\text{H}}^{\text{exc}}$ ($2.1 \cdot 10^{23} \text{ cm}^{-2}$, see Table 2) by two orders of magnitude than, those for the above local absorption model. This is because the absorbed photons have increased energies (by a factor of $1+z$) and thus decreased absorption cross sections in the absorber frame. We over-plotted in Fig. 3 the confidence contours for the fitted $N_{\text{H}}^{\text{exc}}$ and Γ (marked by $z = 4.28$). It should be noted that we have assumed the solar elemental abundances for the absorbing gas. The energy range of $E > 0.7 \text{ keV}$ in which the X-ray photons are absorbed in the ASCA bandpass corresponds to $E \gtrsim 3.5 \text{ keV}$ in the quasar rest frame; at such energies the cross section of photoelectric absorption is dominated by heavy elements, mainly O, Ne, Si, S, Ca, and Fe. Since at high redshifts the metal abundances could be well sub-solar (about 10% or less, e.g. Lu et al. 1996; Pettini et al. 1997; Prochaska & Wolfe 2000), we assumed the metal abundances as $A_Z = 0.1 A_{Z\odot}$ and repeated the fit (using *zvfabs* model in *XSPEC*). The resulting absorption column density becomes as high as $N_{\text{H}}^{\text{exc}} \sim 1.6 \cdot 10^{24} \text{ cm}^{-2}$ (Table 2). Since the true elemental abundances are unknown, the determination of $N_{\text{H}}^{\text{exc}}$ is subject to a large uncertainty, however.

We searched for any redshifted iron K absorption edge by fitting the edge separately from the redshifted absorption model. The best-fit edge energy is $7.2^{(+0.6)}_{(-1.2)} \text{ keV}$; the optical depth at the threshold energy is $\tau = 0.15^{(+0.12)}_{(-0.10)}$, which is consistent the prediction from the fitted $N_{\text{H}}^{\text{exc}}$ ($\tau = 0.26$ for $A_Z = A_{Z\odot}$). However, given the reduction in χ^2 of $\Delta\chi^2 = 1.3$ only, the detection of the iron K edge cannot be justified. The non-detection of a significant iron edge gave no determination of the redshift of the absorber, unfortunately.

It is possible that the absorber is photoionized by the intense radiation from the quasar. A photoionized absorption model (*absori* in *XSPEC*) was fitted to the spectrum, in which the power law X-ray emission of the quasar was taken as the ion-

izing continuum. The result is inconclusive, however. The fit converged at neutral absorption with the best-fit ionization parameter (as defined in Done et al. 1992) $\xi \approx 0$, while ionization of the gas to some degree is allowed, $\xi < 2$ (20) at the 90% (99%) c.l. For sub-solar metal abundances the allowed ξ range becomes lower, $\xi < 0.1$ at the 90% c.l. for $A_Z = 0.1 A_{Z\odot}$. It should be noted that, however, if the relative abundance of iron with respect to other heavy elements is much lower than the solar value, the ionization state is almost unconstrained, though this seems to be an unlikely case. For instance, for $A_Z = A_{Z\odot}$ except $A_{\text{Fe}} = 0.1 A_{\text{Fe}\odot}$, the 90% confidence range for ξ could be as large as 0–1000. This is because the constraint on the ionization state comes largely from the lack of the predicted K-edge features of highly ionized irons in 1.3–1.7 keV in the observer frame.

3.2.2. Redshift dependence

The unknown location of the absorber introduces a large uncertainty in the determination of $N_{\text{H}}^{\text{exc}}$. With the limited low-energy bandpass and energy resolution, ASCA cannot distinguish between local and highly redshifted absorption models. This is because, firstly, these models could have similar spectral shapes of the absorbed continuum in the ASCA band, and secondly, the photon statistics are generally poor at low energies anyway, especially in the case of strong absorption. Leaving the redshift free yielded no statistically significant range in the parameter space, i.e. similar goodness-of-fits for redshifts in the full range of 0–4.28, though there exist a few shallow local minima in the χ^2 distribution (however, see Sect 3.4 for the case when the 0.5–0.7 keV spectral data are included). The dependence of the excess column density on the assumed redshift is shown in Fig. 4, in which the confidence contours are plotted on the $N_{\text{H}}^{\text{exc}} - z$ plane. The required $N_{\text{H}}^{\text{exc}}$ decreases down to $2.5 \cdot 10^{21} \text{ cm}^{-2}$ for $z=0$, as shown in Sect. 3.1. It is also shown that, at a given redshift, $N_{\text{H}}^{\text{exc}}$ is relatively well constrained. It should be noted that these results were obtained by assuming the solar elemental abundances; if the metallicity is significantly sub-solar, the inferred $N_{\text{H}}^{\text{exc}}$ value would increase substantially (see above).

3.3. Other continuum models

Thermal bremsstrahlung model— We also fitted the spectrum with redshifted thermal bremsstrahlung plus local absorption models. For absorption fixed at the Galactic $N_{\text{H}}^{\text{Gal}}$, a source frame temperature as high as $132^{(+41)}_{(-27)} \text{ keV}$ is required. Free fitting the absorption column density gave $T = 55^{(+12)}_{(-9)} \text{ keV}$ and, similarly, a large $N_{\text{H}} = 2.1^{(+0.4)}_{(-0.3)} \cdot 10^{21} \text{ cm}^{-2}$. The resulting goodness-of-fit is the same as that for a power law fit. For such a high temperature, the thermal bremsstrahlung spectrum is indistinguishable from a power law one in the ASCA band.

Broken power law— A convex spectral shape, like what observed in some BL Lac objects, can result in apparent excess absorption when fitted with a power law model. Such spectra are usually parameterized with a broken power law model. Fitting a broken power law with fixed Galactic absorption yielded statistically acceptable fit, $\chi^2 = 190$ for 209 degrees of freedom (d.o.f.); in spite of one more free parameter, the χ^2 is somewhat worse than those for the power law with excess absorption models. The resulting break energy of $9 \pm 1 \text{ keV}$ (in the quasar frame) is higher than those found for the X-ray spectra of BL Lac objects (a few keV or less, e.g. Barr et al. 1988;

Madejski et al. 1991). Leaving the absorption N_{H} free improved the fits slightly ($\Delta\chi^2 = 3$), and yielded similar values for the high- and low-energy photon indices (Table 2), and a $N_{\text{H}} \sim 2.8(\pm 0.7) 10^{21} \text{ cm}^{-2}$ significantly larger than the Galactic value. Such a model is effectively consistent, within the uncertainties of the fitted parameters, with the absorbed power law models—the best-fit models as shown above.

3.4. Effect of the low-energy end data: excess absorption?

As shown above, the 0.7–9.5 keV spectrum can be similarly well modeled by either the power law with (local or redshifted) excess absorption models or the broken power law continuum with Galactic absorption. Since these models show increasing spectral divergence toward low energies, the omitted 0.5–0.7 keV SIS data, even in the presence of the calibration uncertainties, might be useful for discriminating between these models. Here we examine the effect of the excluded 0.5–0.7 keV SIS data (two bins after spectral binning) on the obtained results in two ways.

Firstly, we extrapolated the above best fits for various models obtained with the 0.7–9.5 keV spectrum down to 0.5 keV for SIS and compared the model values with the data. For all the models, deficits of the observed count rate in these energy bins were always found for both SIS0 and SIS1, which might be a result of the above systematic effect, or mismatched models, or both. We examined the consistency of the observed 0.5–0.7 keV count rates with the current models by evaluating the F -statistic F , which basically measures the change in χ^2 with the change of the degrees of freedom in fitting. (For a F as large as exceeding the F_{cr} which corresponds to a certain probability level $P(F_{\text{cr}})$, the chance probability under the model hypothesis is as small as $P < P(F_{\text{cr}})$). For models of the power law with redshifted absorption, with local absorption, and the broken power law with Galactic absorption, we found the χ^2 increments of $\Delta\chi^2 = 4, 12, \text{ and } 30$ for two additional d.o.f., and the calculated $F=2.1, 6.4, 14.4$, and the probability levels $P > 5\%, < 1\%, < 1\%$, respectively. Thus, regardless of the SIS calibration uncertainty, the second and the third models do not agree with the 0.5–0.7 keV data at high confidence levels. This can be understood as the redshifted absorption model, with its large absorption N_{H} , predicts the strongest low-energy spectral cutoff, i.e. the least count rates in 0.5–0.7 keV.

It has been claimed that at 0.6 keV the decrease of the efficiencies can be as much as 40% for SIS1 in the current observations (compared with GIS, ASCA Guest Observer Facility web page). We took this systematic effect into account by lowering the model values in the 0.5–0.7 keV bin by 40% for (conservatively) both SIS0 and SIS1, and repeated the above testing. We have $\Delta\chi^2 = 1, 5, \text{ and } 9.5$ for the above three corresponding models, respectively. This means while the first and the second models give the best and marginal consistencies with the 0.5–0.7 keV data ($F=0.6$ and 2.7), respectively, the broken power law model still disagrees with the included data at high confidence level ($F=5, P < 1\%$).

Secondly, we tried to compensate the SIS calibration uncertainties by decreasing the detecting efficiencies in the 0.5–0.7 keV band by 20% for SIS0 and by 40% for SIS1, and fitted the SIS+GIS spectra in the *whole* 0.5–9.5 keV band using the ‘corrected’ SIS calibration files. This resulted in the best-fit model being the power law with excess absorption in the quasar frame, with the goodness-of-fit ($\chi^2=190$ for 212 d.o.f.) improved slightly over the power law with local absorption

model ($\chi^2=193$ for 212 d.o.f.), and considerably over the broken power law with Galactic absorption model ($\chi^2=197$ for 211 d.o.f.). The fitted spectral parameters are similar to those obtained by fitting the 0.7–9.5 keV spectra. It is interesting to note that, for the excess absorption models, the redshift of the absorber could be free fitted as $z = 4.2_{-0.5}^{+0.6}$ (90% c.l.); however, this result is only suggestive given the non-uniform efficiency loss over the 0.5–0.7 keV band and the less strict treatment here.

We conclude that the broken power law with Galactic absorption model gives a poor description to the observed low-energy spectrum down to 0.5 keV, in comparison with the (redshifted) excess absorption model. Furthermore, the SIS data in the 0.5–0.7 keV range are better described by the absorption model with the absorber being at or close to the quasar redshift than the local absorption model.

4. TEMPORAL PROPERTIES

The 67-hour duration of the observation corresponds to ~ 12.7 hours in the quasar frame, which is short for quasar timing analysis. The X-ray variability was searched for from the background-subtracted light curve by using the packages provided in the FTOOLS. No statistically significant variations were found in both the co-added SIS and GIS light curves, as well as in the combined SIS+GIS light curve. It is noted, however, that a marginal, small amplitude variation could probably be present in the first half of the duration (χ^2 test, $\chi^2 = 15$ for 9 d.o.f., a probability level of 0.09).

We compared our results with the RASS flux by extrapolating the best-fit model down to 0.1 keV. The predicted count rate in the ROSAT 0.1–2.4 keV band is 0.02 cts s^{-1} , consistent with the RASS measurement $0.035 \pm 0.011 \text{ cts s}^{-1}$ (Zickgraf et al. 1997) within the errors. Thus, no significant flux variation was found by comparing the two observations of about 2 years apart in the source rest frame. It should be noted that, in the ROSAT soft 0.1–0.41 keV band, only ~ 0.1 source count is predicted for the 424 second RASS exposure due to the strong absorption of soft X-rays, in contrast to the observed ~ 2 counts (a counting statistical probability of 3% only). This may imply the latter to be either of background fluctuations, or source photons scattered off the absorbing medium down to the soft X-ray energies.

5. DISCUSSION

We have shown that the X-ray spectrum of RX J1028.6-0844 exhibits a low-energy cutoff much stronger than that expected from the Galactic absorption. Though both, the power law with excess absorption and the broken power law with Galactic absorption models give acceptable fits to the spectra, the former is favored over the latter based on the fitting statistics. On the other hand, the power law model has been found to be a characteristic of the intrinsic X-ray continuum emission of FSRQ over a wide range of redshift. We thus suggest that the broken power law model seems to be an unlikely case, though it cannot be ruled out confidently, and the observed excess spectral cutoff is most likely caused by absorption of the soft X-ray photons from the quasar. This explanation is much natural in the light of what has been established in the redshift range of around 2 to 3—excess X-ray absorption is common in radio quasars, and extends this behavior up to redshift above 4 (two out of the three objects with well determined X-ray spectra). We consider this scenario only and discuss its implications in below.

5.1. The absorber

The derived column density of the excess absorption (hereafter denoted simply as N_{H}) is among the largest⁸ ever found for high- z radio quasars, which imposes a strong observational constraint on the nature of the absorbing material. In addition, any satisfactory absorption models should be able to accommodate the absorber to the following facts: (a) the relatively well constrained $N_{\text{H}} - z$ relation (Fig 4), though with some uncertainties introduced from the unknown metallicity; (b) being nearly neutral or moderately ionized, $\xi < 2$ at the 90% c.l. (unless the iron abundance relative to other heavy elements is abnormally sub-solar; see above); (c) no strong absorption beyond the Lyman limit, as indicated by both the optical (UV in the source frame) spectrum and the measured B -magnitude (emitted at 834 Å) in Zickgraf et al. (1997); and similarly, (d) no indication of heavy dust extinction; (e) if the X-ray emission is mainly from the jet (a likely case, see Sect. 5.2), the absorber must lie outside the jet from the nucleus or around the jet. Several possible origins of the X-ray absorption of high- z radio quasars have been proposed (see Elvis et al. 1994, 1998), such as damped Ly α systems, intracluster gas, and the boundary layer between the jet and surrounding medium. We discuss in below the implications of our results for the possible absorbers of both intervening and intrinsic origins.

5.1.1. Cosmological intervening material?

An inspection of the optical image of the quasar field obtained by Zickgraf et al. (1997) suggests readily an absorber candidate: an extended, faint (speculative) spiral galaxy, which lies $\sim 7''$ away from the quasar and seems not highly inclined given the estimated optical axes of $\sim 5'' \times 3''$. The presumed H I gas disk/halo might intersect the quasar line-of-sight at a transverse distance of from a few kpc ($z \ll 1$) to several tens kpc ($z \sim 1$). If this object is indeed a spiral galaxy, absorption of the quasar X-rays by its H I gas is unavoidable. The question is whether the amount of the absorbing gas can account for the large column density derived here. Observational evidence for X-ray absorption due to galactic H I disk/shell has just emerged in a few systems (Elvis et al. 1997; Yuan and Brinkmann 1999), but the measured N_{H} are relatively low (several times 10^{20} cm^{-2}). We tried to assess quantitatively the amount of such possible absorption. We estimated the averaged N_{H} of the anticipated H I gas in this galaxy from its optical brightness, by making use of the galactic H I - mass and luminosity relation and the distance-independent scaling $N_{\text{H}} \simeq 10^{20} (M_{\text{HI}}/L_{\text{B}}) 10^{0.4(27-\mu_{\text{B}})}$ (Disney and Banks 1997), where $M_{\text{HI}}/L_{\text{B}}$ is the H I -mass to light ratio in units of M_{\odot}/L_{\odot} , and μ_{B} the B -band surface brightness averaged over the H I disk. Adopting the measured $m_{\text{B}} = 20.2 \pm 0.5$, we found a conservative $\mu_{\text{B}} \sim 25.2$ (Galactic extinction corrected), which is averaged over the solid angle confined by an ellipse with the inferred axis ratio and intersecting the quasar sight-line. This led to an averaged $N_{\text{H}} \sim 5.2_{-1.9}^{+3.1} 10^{20} (M_{\text{HI}}/L_{\text{B}}) \text{ cm}^{-2}$, where the quoted errors are from the uncertainty of m_{B} . To match the excess absorption N_{H} of $2.5_{-0.4}^{+0.5} 10^{21} \text{ cm}^{-2}$ ($z = 0$ and $A_{\text{Z}} = A_{\text{Z}\odot}$), a $M_{\text{HI}}/L_{\text{B}}$ ratio as high as 4–5 is needed; this seems to be unlikely as spirals being found to have $M_{\text{HI}}/L_{\text{B}} \lesssim 1$ regardless of the morphological type (e.g. Kamphuis et al. 1996). Moreover, the true N_{H} at the site of the quasar sight-line might be even lower than the averaged value as the H I surface density drops rapidly outward from the center. We therefore suggest that this galaxy is probably responsible for part of the X-ray absorption,

but it is unlikely—though we cannot rule it out—to be able to account for the *total* absorption opacity. After subtracting the plausible contribution of this galaxy (assuming $M_{\text{HI}}/L_{\text{B}} \lesssim 1$), an excess column density of $N_{\text{H}} \gtrsim 2.0_{-0.4}^{+0.5} 10^{21} \text{ cm}^{-2}$ ($z = 0$ and $A_{\text{Z}} = A_{\text{Z}\odot}$) may remain unaccounted for.

Such a large amount of absorption seems not to be easily explained by the general damped Ly α systems (DLA), neutral hydrogen reservoirs with the largest column density (N_{HI}) known in the universe. Although DLA may have the distribution of N_{HI} reaching a few times 10^{21} cm^{-2} at its high end, the steep distribution function with a power law index of -3 renders such systems to be extremely rare (Wolfe et al. 1995, Zwaan et al. 1999). The deficit of column density is even severe regarding the substantially sub-solar metal abundances ($A_{\text{Z}} < 0.1A_{\text{Z}\odot}$) of DLA, even at $z \simeq 0$ (Miller et al. 1999), which require N_{H} to be well above 10^{22} cm^{-2} in order to produce the observed absorption. Although the true total hydrogen column density N_{H} could be somewhat higher than N_{HI} considering a possible ionization fraction of H, the correction should not be large as gases in DLA are believed to be mainly neutral (Wolfe 1993). A detailed study by O’Flaherty and Jakobsen (1997) incorporating absorber statistics confirmed the extremely low detectability of high- N_{H} intervening systems; the chance probability to have a DLA with $N_{\text{H}} \gtrsim 10^{21} \text{ cm}^{-2}$ on the line-of-sight to a high- z quasar is less than a few percent. This probability is even lower considering that any DLA systems, if do produce the absorption, are most likely at low redshifts so as to avoid the otherwise much higher X-ray N_{H} required (Fig. 4). The non-detection of a DLA in the optical spectrum obtained by Zickgraf et al. (1997) places an upper limit on the redshift of any possible DLA as ~ 2.5 . Therefore, the likelihood of the absorption being caused by cosmologically intervening material is regarded to be low.

5.1.2. Intrinsic absorber?

Alternatively, the excess absorption might take place intrinsically close to the quasar. This seems to be plausible in the light of the statistical arguments for high- z radio-quiet quasars showing no excess absorption. The inferred absorption column density in the quasar rest frame then reaches the highest ever found among this type, $\sim 2 \cdot 10^{23} \text{ cm}^{-2}$ ($\gtrsim 1.7 \cdot 10^{23} \text{ cm}^{-2}$ corrected for the possible foreground galactic absorption assuming the expected $M_{\text{HI}}/L_{\text{B}} \lesssim 1$, see Sect. 5.1.1) or even higher up to $\sim 10^{24} \text{ cm}^{-2}$ if $A_{\text{Z}} \lesssim 0.1A_{\text{Z}\odot}$. Such thick gas can not be easily explained by the known mass components. This result strengthens the tentative, apparent trend of the increasing N_{H} of excess absorption in radio quasars with the increase of redshift, which might have interesting consequences for understanding the evolution of quasars and, probably, the formation of the cosmic structure.

One immediate problem, which seems to be common among objects of this type (Elvis et al. 1994), arises as the apparent inconsistency between the X-ray and optical data: the thick gas, if contains dust similar to that of our Galaxy in both composition and content, would have blocked almost all the optical/UV light of the quasar believed to originate from the central region, e.g. $A(\lambda 1230\text{Å})=40$ (Seaton 1979) for the observed R -magnitude. Though this problem may be relieved by a likely extremely low dust content or different dust compositions at high redshift (see Elvis et al. 1994 for a discussion), the lack of strong Lyman limit absorption remains a concern. A rough estimate of $\tau_{912\text{Å}} \lesssim 1$ from the optical spectrum in Zickgraf et

⁸Similar amounts of excess absorption were also reported in S5 0014+81 (Cappi et al. 1997) and PKS 0528+134 (Reeves et al. 1997).

al. (1997) suggests the absorber to be highly ionized, $N_{\text{H I}}/N_{\text{H}} \lesssim 10^{-6}$ (taking the conservative value of $N_{\text{H}} = 1.7 \times 10^{23} \text{ cm}^{-2}$). This ionization state requires the dimensionless ionization parameter $U \gtrsim 5$ (U is defined as the hydrogen-ionizing photon-to-electron number density ratio) for the typical AGN ionizing continuum, or, when converted to ξ , $\xi \gtrsim 250$; assuming the ionizing continuum as the extrapolation of the observed flat power law with $\Gamma \simeq 1.7$ requires $\xi \gtrsim 370$. However, we found $\xi \lesssim 2$ (20) at the 90% (99%) c.l. from the X-ray data. One natural explanation would be that the UV continuum emitting region is only partially or not covered by the X-ray absorber. If this is the case, special geometry of the absorbing gases may be required; for instance, the gas might be ambiently local to the jet if the X-rays are of jet emission (constraint e). Again, it should be noted that, if the gas has iron-poor metallicity in comparison to the solar one, a higher ionization state cannot be ruled out.

Interestingly, Elvis et al. (1994) related the X-ray absorption of quasars up to $z \sim 3$ to cooling flows of the possible host clusters of galaxies, though the existence of relaxed clusters at such high redshifts is unknown. If we take this hypothesis and extend the redshift up to $z \sim 4$ for the case of RXJ1028.6-0844, its large N_{H} value in comparison to those found from X-ray absorption in low-redshift clusters ($\sim 10^{21} \text{ cm}^{-2}$, White et al. 1991) would imply an extremely strong cooling flow. The mass of the cooled gas reaches $\sim 3 \times 10^{13} R_{100}^2 M_{\odot}$ for a conservative $N_{\text{H}} = 10^{23} \text{ cm}^{-2}$, where R_{100} is the cooling flow radius in units of 100 kpc. For $R_{100} \sim 1$ as typically found in low- z clusters, this means a cooled mass of $\sim 3 \times 10^{13} M_{\odot}$, and a mass cooling rate $\gtrsim 3 \times 10^4 M_{\odot} \text{ yr}^{-1}$ given the short life-time of the system of less than 10^9 years. Such a cooling flow almost approaches the ‘maximal cooling flow’ in which the cooling time is comparable with the gravitational free-fall time (Fabian 1994). Though these numbers will be somewhat reduced for a likely clumpy distribution of the cooled gas, a cooling flow stronger than those in nearby clusters is suggested.

It has also been noted that the massive ($\sim 10^{14} M_{\odot}$) neutral hydrogen cloud at $z=3.4$ reported by Uson et al. (1991) could be a possible origin of X-ray absorption. The gas cloud was detected via both absorption and emission lines at the radio 21 cm wavelength, and was interpreted as indications of a proto-cluster of galaxies. The H I column density derived from the absorption line is $4.4 \times 10^{18} (T_s/\text{K}) \text{ cm}^{-2}$ (T_s the spin temperature of H I); the mean surface mass density was estimated from the emission line as $\sim 48 M_{\odot} \text{ pc}^{-2}$ (Uson et al. 1991), which corresponds to an averaged column density $N_{\text{H I}} \sim 5.7 \times 10^{21} \text{ cm}^{-2}$. If such a system is responsible for the X-ray absorption in RXJ1028.6-0844, the gas must be hot with $T_s > 10^4 \text{ K}$, and/or somewhat ionized, $N_{\text{H}}/N_{\text{H I}} > 10$; these lower limits will be further raised up for $A_z < A_{z\odot}$. Thus, the inferred T_s and/or total gas mass are likely exceeding 10^4 K and $3 \times 10^{14} M_{\odot}$, respectively, the values proposed for a “Zel’dovich pancake” (Sunyaev and Zel’dovich 1975).

If the quasar X-rays are dominated by jet emission, the absorption may be caused by intimately jet-linked material. Such a scenario explains naturally the lack of UV absorption and reddening, which seems to be a commonplace for high- z radio quasars showing excess X-ray absorption. It is of particular interest to relate the X-ray absorption with the optical-radio ‘alignment effect’ found in high- z radio galaxies, as noted in Elvis et al. (1998). This effect is the alignment of the extended, polarized optical emission with the radio axes (e.g. McCarthy 1993), which is thought to be of (dust) scattering

and/or star-formation origin. A class of dust scattering models advocates the existence of gas-dust clouds embedded in a multi-phase boundary layer formed (from interaction) between the jet and ambient medium (e.g. De Young 1998). Although such a jet environment is largely uncertain, it is interesting to note the following order-of-magnitude estimation. We consider a specific set of model parameters which was adopted so as to roughly satisfy the physical condition and observations as proposed in De Young (1998): gas density $n=10\text{--}100 \text{ cm}^{-3}$, cloud size $R_c \sim 100 \text{ pc}$. We assume the boundary layer containing one layer of similar clouds, i.e. its height is characterized by the size of the clouds R_c . Consider an X-ray photon emitted from the jet with an angle θ with respect to the jet axis in the observer frame; for FSRQ, θ is small, $\theta \lesssim 10^\circ$. The average number of the clouds that the photon is expected to encounter before it escapes out of this ‘cocoon’ is $N_{\text{enc}} = R_c/(\sin\theta d_c)$, where d_c is the mean distance between two neighboring clouds. If the clouds are abundant enough, $d_c/R_c \lesssim (\sin\theta)^{-1}$, N_{enc} reaches unity ($N_{\text{enc}} \gtrsim 1$) and results in X-ray absorption with almost a full coverage as viewed from the observer. The column density is then $N_{\text{H}} \sim nR_c N_{\text{enc}} = 3N_{\text{enc}} 10^{21\text{--}22} \text{ cm}^{-2}$. Thus, for only one encounter on average ($N_{\text{enc}}=1$) the resulting N_{H} is sufficient to account for the X-ray column densities found in most of the excess absorption quasars. To reach $N_{\text{H}} \sim 10^{23} \text{ cm}^{-2}$ in RXJ1028.6-0844, an increase in N_{enc} up to several encounters is required; this may be achieved by a rather small viewing angle to the jet θ , and/or an increased cloud number density (reduced d_c). For such a model, the presence of X-ray absorption in radio quasars might be governed by the formation of such a boundary layer, for which cosmic evolution is needed to explain the difference at high and low redshifts.

5.2. The quasar

The 2–50 keV luminosity of $2.6 \times 10^{47} \text{ erg s}^{-1}$, after correction for the total absorption, makes RXJ1028.6-0844 one of the most luminous quasars. Furthermore, if $A_z \lesssim 0.1 A_{z\odot}$, we have $N_{\text{H}} \gtrsim 10^{24} \text{ cm}^{-2}$ and the Thomson depth $\tau_{\text{Th}} \simeq 1.2\sigma_{\text{Th}}N_{\text{H}}$ reaches unity for photons with energies above a few keV (so that electrons bound to atoms can be treated as free); electron scattering becomes non-negligible and actually dominating the opacity for photons with $E \gtrsim 5 \text{ keV}$. An additional correction for such electron scattering opacity would raise the 2–50 keV luminosity at least a few times higher, perhaps approaching $10^{48} \text{ erg s}^{-1}$. This will make the quasar one of the most luminous steady objects if the radiation is isotropic.

Fig. 5 shows the spectral energy distribution (SED) for RXJ1028.6-0844, with the X-ray luminosity corrected for the total absorption. The UV luminosities (L_{UV}) are somewhat uncertain due to the unknown dust extinction possibly imposed by the X-ray absorber. For a comparison, also plotted are L_{UV} (open circles) for one extreme case in which the absorption is solely attributed to a local intervening (galactic) absorber with the Galactic dust-to-gas ratio; L_{UV} then reaches $10^{47} \text{ erg s}^{-1}$. The situation is less clear for the case of intrinsic absorption, as discussed above; in any case L_{UV} must be no less than the observed values for which only the correction for the Galactic reddening was applied (filled dots).

It has been pointed out by Fabian et al. (1999) that this object (and the other two $z > 4$ quasars) is distributed somewhat apart from the bulk of nearby blazars on the $\alpha_{\text{rx}} - \alpha_{\text{ox}}$ and $\alpha_{\text{ro}} - \alpha_{\text{ox}}$ planes, where α_{ro} , α_{rx} , and α_{ox} are the so-called broad band

effective spectral indices⁹ spanning between the radio, optical, and X-ray wavebands, respectively. For RX J1028.6-0844, this might be, at least partly, a consequence of the optical/UV extinction imposed by the obscuring matter. The intrinsic α_{ro} and α_{ox} would flatten and steepen, respectively, and this would shift the object toward or into the bulk distribution of FSRQ and radio-selected BL Lac objects in the $\alpha_{\text{ro}} - \alpha_{\text{rx}} - \alpha_{\text{ox}}$ parameter space (see Fig. 4 in Fabian et al. 1999), depending on the amount of dust extinction. For example, assuming local absorption and the dust-to-gas ratio similar to the Galactic one, we found¹⁰ intrinsic $\alpha_{\text{ro}}=0.56$, $\alpha_{\text{rx}}=0.75$, and $\alpha_{\text{ox}}=1.11$.

Both, the broad band SED and the extreme X-ray luminosity suggest that RX J1028.6-0844 might be a blazar type object; its high radio power is also of typical FSRQ. We may thus come to the suggestion that all these three $z > 4$ quasars, regardless of the strong X-ray absorption of RX J1028.6-0844, are of the same class, and the X-rays are thought to be emitted via inverse Compton radiation (Jones et al. 1974). Similar to GB 1428+4217 as discussed in Fabian et al. (1999), the optical/UV luminosity of RX J1028.6-0844 might not be dominated by the beamed non-thermal emission, but originate from accretion process; if this is true, the high luminosity would imply that black holes as massive as $10^8 - 10^9 M_{\odot}$ have formed within less than 1 billion years in the early stages of the universe.

Owing largely to its low-energy cutoff, the X-ray spectrum of the quasar is consistent with that of the cosmic X-ray background (CXB) in the 0.6–10 keV ASCA band, $\Gamma=1.4$ power law (Gendreau et al. 1995) or $kT=40$ keV bremsstrahlung (3–50 keV, Marshall et al. 1980) with Galactic absorption (fits with the parameters fixed at these values resulted in reduced $\chi^2=1.1$ and 1.0 for 212 d.o.f., respectively). However, this type of objects appears simply too rare to make significant contribution to the CXB.

Finally, it is noted that the $z=4.3$ quasar 1508+5714 revealed a high rest-frame temperature 93^{+40}_{-24} keV (90% errors, Moran & Helfand 1997) when fitted with a redshifted bremsstrahlung with Galactic absorption model. This value is similar to that found for RX J1028.6-0844 of 132^{+41}_{-27} keV, which apparently resulted from the low-energy cutoff in its spectrum. Such a comparison suggests possible excess absorption in 1508+5714 too, of which the ASCA observation might not be deep enough to allow a detection. The 90% upper limit on the excess absorption N_{H} at the quasar redshift was given as $1.3 \times 10^{22} \text{ cm}^{-2}$ (Moran and Helfand 1997).

6. SUMMARY

We present the broad band 3–50 keV (source rest frame) X-ray observation of the quasar RX J1028.6-0844 at $z = 4.28$. The spectrum, with its unprecedented high quality among observations of objects at similar redshifts, reveals an evident, substantial low-energy cutoff in excess of that due to Galactic absorption. The spectrum is best modeled by a power law with excess photoelectric absorption model, yet a broken power law with Galactic absorption cannot be ruled out. We suggest the excess absorption to be the most likely explanation, considering the spectral data at the low-energy end. The column density of the absorber, depending on its redshift and metallicity, ranges from $2.5 \times 10^{21} \text{ cm}^{-2}$ for local absorption up to $2.1 \times 10^{23} \text{ cm}^{-2}$ (solar metallicity) or $1.6 \times 10^{24} \text{ cm}^{-2}$ (10% solar metallicity) for absorption at the quasar redshift. It has to be noted there may be a systematic uncertainty in the determination of the column density, which tends to overestimate the absorption; however, we suggest this effect to be small and negligible in comparison to the statistical uncertainties. We attribute a possible part of the absorption opacity to a putative foreground spiral galaxy; the remaining absorption, most likely the majority part, seems not to be easily explained by cosmological intervening systems. Future observations with XMM and Chandra would be able to measure the redshift and other parameters of the absorber by detecting possible iron absorption edges above 7 keV.

The unabsorbed quasar continuum is well described by a simple power law with $\Gamma = 1.67^{+0.07}_{-0.04}$ extending up to 50 keV in the source rest frame. The absorption corrected luminosity reaches as high as $2.6 \times 10^{47} \text{ erg s}^{-1}$, regardless of possible electron scattering effect. No statistically significant X-ray flux variations were found during the relatively short observational interval, neither by a comparison with the early ROSAT Survey observation. Considering its extreme apparent luminosities in the X-ray and radio bands, as well as the broad band SED, we suggest RX J1028.6-0844 to be a blazar type object, similar to the other two $z > 4$ quasars observed with broad band X-ray spectroscopy.

We thank all the members of ASCA team for making the observations and data analysis possible. We would also like to thank the referee for a careful reading of the manuscript and the useful comments which helped to improve the paper. W.Y. acknowledges the STA fellowship and hospitality at NASDA. This research has made use of the NASA/IPAC Extragalactic Database (NED), which is operated by the JPL, Caltech, under contract with the National Aeronautics and Space Administration.

REFERENCES

- Barr, P., Giommi, P., Maccagni, D., 1988, *ApJ*, 324, 11
 Bechtold, J., Elvis, M., Fiore, F., et al., 1994, *AJ*, 108, 759
 Boller, Th., Fabian, A. C., Brandt, W. N., and Freyberg, M. J., 2000, *MNRAS*, in press
 Brinkmann, W., Yuan, W., Siebert, J., 1997, *A&A*, 319, 413
 Cappi, M., Matsuoka, M., Comastri, A., et al., 1997, *ApJ*, 478, 492
 De Young, D. S., 1998, *ApJ*, 507, 161
 Dickey, J. M., & Lockman, F. J. 1990, *ARA&A* 28, 215
 Disney, M. J., & Banks, G., 1997, *PASA*, 14, 69
 Done, C., Mulchaey, J. S., Mushotzky, R. F., Arnaud, K. A., 1992, *ApJ*, 395, 275
 Dotani, T., et al., 1996, *ASCA News Letter*, 4, 3
 Elvis, M., Fiore, F., Wilkes, B., McDowell, J., Bechtold, J., 1994, *ApJ*, 422, 60
 Elvis, M., Fiore, F., Giommi, P., Padovani, P., 1997, *MNRAS*, 291, L49
 Elvis, M., Fiore, F., Giommi, P., Padovani, P., 1998, *ApJ*, 492, 91
 Fabian, A. C., 1994, *ARA&A*, 32, 277
 Fabian, A. C., Iwasawa, K., Celotti, A., et al., 1998, *MNRAS*, 295, L25
 Fabian, A. C., Celotti, A., Pooley, G., et al., 1999, *MNRAS*, 308, L6
 Fiore, F., Elvis, M., Giommi, P., Padovani, P., 1998, *ApJ*, 492, 79
 Gendreau, K. C., Mushotzky, R. F., Fabian, A. C., 1995, *PASJ*, 47, L5
 Jones, T. W., O'Dell, S. L., Stein, W. A., 1974, *ApJ*, 188, 353
 Kamphuis, J. J., Sijbring, D., van Albada, T. S., 1996, *A&AS*, 116, 15
 Kubo, H., Makishima, K., Takahashi, T., 1997, *MNRAS*, 287, 328
 Lawson, A. J. and Turner, M. J. L., 1997, *MNRAS*, 288, 920
 Lu, L., Sargent, W.L.W., Barlow, T. A., Churchill, C. W., Vogt, S., 1996, *ApJS*, 107, 475

⁹Defined as $\alpha_{\text{ro}} = -\log(L_{\text{o}}/L_{\text{r}}) / \log(\nu_{\text{o}}/\nu_{\text{r}})$, $\alpha_{\text{rx}} = -\log(L_{\text{x}}/L_{\text{r}}) / \log(\nu_{\text{x}}/\nu_{\text{r}})$, and $\alpha_{\text{ox}} = -\log(L_{\text{x}}/L_{\text{o}}) / \log(\nu_{\text{x}}/\nu_{\text{o}})$, where L_{r} , L_{o} , and L_{x} are the monochromatic luminosities at the radio ν_{r} , optical ν_{o} , and X-ray ν_{x} bands, respectively.

¹⁰The radio, optical and X-ray luminosities are calculated at 5 GHz, 5500 Å and 1 keV, and an optical spectral index of -0.7 is assumed for K-correction.

- Madejski, G. M., Mushotzky, R. F., Weaver K. A., Arnaud, K. A., Urry, C. M., 1991, *ApJ*, 370, 198
- Marshall, F. E., Boldt, E. A., Holt, S. S., et al., 1980, *ApJ*, 235, 4
- Matsuoka, M., Wang, T., Kubo, H., et al., 1999, in *Highlights in X-ray Astronomy*, ed., Aschenbach, B., and Freyberg, M., (MPE Report 272), 236
- McCarthy, P. J., 1993, *ARA&A*, 31, 639
- Miller, E. D., et al., 1999, *ApJ*, 510, L95
- Moran, E. C., and Helfand D. J., 1997, *ApJ*, 484, L95
- Morrison, R., and McCammon, D., 1983, *ApJ*, 270, 119
- O’Flaherty, K. S. and Jakobsen, P., 1997, *ApJ*, 479, 673
- Otrupcek, R. E. and Wright, A. E., 1991, *PASA*, 9, 170
- Pettini, M., Smith, L. J., King, D. L., Hunstead, R. W., 1997, *ApJ*, 486, 665
- Prochaska J. X. and Wolfe, A. W., 2000, *astro-ph/0002513*
- Reeves, J. N., Turner, M. J. L., Ohashi, T., Kii, T., 1997, *MNRAS*, 292, 468
- Schartel, N., Komossa, St., Brinkmann, W., et al., 1997, *A&A*, 320, 421
- Seaton, M. J., 1979, *MNRAS*, 187, 73
- Serlemitsos, P., Yaqoob, T., Ricker, G., et al., 1994, *PASJ*, 46, L43
- Siebert, J., Matsuoka, M., Brinkmann, W., et al., 1996, *A&A*, 307, 8
- Sunyaev, R. A. and Zel’dovich, Ya. B., 1975, *MNRAS*, 171, 375
- Tanaka, Y., Inoue, H., Holt, S. S., 1994, *PASJ*, 46, L37
- Uson, J. M., Bagri, D. S., Cornwell, T. J., 1991, *Phy. Rev. Lett.*, 67, 3328
- White, D. A., Fabian, A. C., Johnstone, R. M., Mushotzky, R. F., Arnaud, K. A., 1991, *MNRAS*, 252, 72
- Wilkes, B. J., Elvis, M., Fiore, F., et al., 1992, *ApJ*, 393, L1
- Wolfe, A. M., 1993, in *Relativistic Astrophysics and Particle Cosmology*, ed. C. W. Akerlof & M. A. Srednicki (New York: Academy of Sciences), 281
- Wolfe, A. M., Lanzetta, K. M., Foltz, C. B., Chaffee F. H., 1995, *ApJ*, 454, 698
- Yaqoob, T., & ASCA team, 2000, *ASCA GOF Calibration Memo* (ASCA-CAL-00-06-01, v1.0)
- Yuan, W. and Brinkmann, W., 1999, in *Highlights in X-ray Astronomy*, ed., Aschenbach, B., and Freyberg, M., (MPE Report 272), 240
- Zickgraf, F.-J., Voges, W., Krautter, J., et al., 1997, *A&A*, 323, L21
- Zwaan, M. A., Verheijen M. A. W., Briggs, F. H., 1999, *PASA*, 16, 100

TABLE 1
ASCA OBSERVATION AND DATA SCREENING

Item	SIS0	SIS1	GIS2	GIS3
Elevation angle ^a	15°/30°	15°/25°	15°	15°
C.O.R. ^b	8	8	8	8
Exposure (sec)	59061	60533	55085	55090
Counts ^c	2179	1831	1620	1807
Background counts ^d	675 (1.14)	606 (1.08)	657 (2.0)	786 (2.0)
Net count rates ^e	2.54±0.10	2.02±0.09	1.74±0.08	1.85±0.09

^aFor SIS the second number refers to the bright Earth elevation angle.

^bMagnetic cutoff rigidity in GeV/c

^cOverall counts from the source extracting region

^dBackground counts normalized to the source extracting region, which are the extracted background counts divided by the ratio of the background-to-source region areas (in bracket).

^eBackground subtracted count rate in units of 10⁻² cts s⁻¹ in the 0.6–10 keV band for SIS and the 0.7–10 keV band for GIS.

TABLE 2
RESULTS OF X-RAY SPECTRAL FITS

Detector	Power law + local neutral absorption			χ^2/dof
	N_{H}^{a}	Γ	norm. ^b	
GIS	0.0459 (fix)	1.51 ± 0.06	1.98 ± 0.12	110/100
SIS0+SIS1	0.0459 (fix)	1.24 ± 0.04	1.38 ± 0.06	102/112
SIS+GIS	0.0459 (fix)	1.34 ± 0.03	1.69 ± 0.07	221/211
GIS	$0.30^{+0.12}_{-0.10}$	$1.76^{+0.12}_{-0.07}$	$2.81^{+0.51}_{-0.42}$	104/99
SIS0+SIS1	$0.26^{+0.06}_{-0.05}$	1.56 ± 0.09	$2.06^{+0.24}_{-0.17}$	84/111
SIS+GIS	$0.30^{+0.05}_{-0.04}$	$1.67^{+0.07}_{-0.04}$	$2.61^{+0.24}_{-0.21}$	187/210
Power law + excess absorption at $z = 4.28$ and $N_{\text{H}}^{\text{Gal}}$ (SIS+GIS)				
$A_{\text{Z}}/A_{\text{Z}\odot}$	$N_{\text{H}}^{\text{exc}}$	Γ	norm.	χ^2/dof
1.0 (fix)	$21.1^{+5.3}_{-4.2}$	$1.72^{+0.10}_{-0.07}$	$2.86^{+0.40}_{-0.26}$	187/210
0.1 (fix)	156^{+31}_{-26}	$1.72^{+0.04}_{-0.08}$	2.81 ± 0.50	186/210
Bremsstrahlung + local neutral absorption (SIS+GIS)				
redshift	N_{H}	T (keV)	norm. ^c	χ^2/dof
4.276 (fix)	0.0459 (fix)	$131.7^{+40.5}_{-26.7}$	3.53 ± 0.16	210/211
4.276 (fix)	$0.21^{+0.04}_{-0.03}$	$54.7^{+12.2}_{-9.2}$	$3.75^{+0.14}_{-0.16}$	187/210
Broken power law + local neutral absorption (SIS+GIS)				
$E_{\text{break}}^{\text{d}}$	N_{H}	Γ_{low}	Γ_{high}	χ^2/dof
$1.7^{+0.2}_{-0.3}$	0.0459 (fix)	$0.70^{+0.18}_{-0.27}$	$1.58^{+0.08}_{-0.11}$	190/209
$2.0^{+\text{inf}}_{-\text{inf}}$	0.28 ± 0.07	$1.58^{+2.48}_{-0.38}$	$1.67^{+0.34}_{-0.10}$	187/208

^aColumn density of hydrogen in units of 10^{22} cm^{-2}

^bNormalization in units of $10^{-4} \text{ photons s}^{-1} \text{ cm}^{-2} \text{ keV}^{-1}$ at 1 keV. For joint SIS+GIS fits, the values given are of GIS, and those of SIS are less by within 10% in general.

^cNormalization as given in XSPEC in units of $10^{-14}/(4\pi D^2) \int n_e n_{\text{H}} dV$, where D is the luminosity distance to the source (cm) and n_e and n_{H} the electron and hydrogen densities (cm^{-3}), respectively.

^dThe break energy of broken power law in keV. Un-specified uncertainties mean the value is unconstrained.

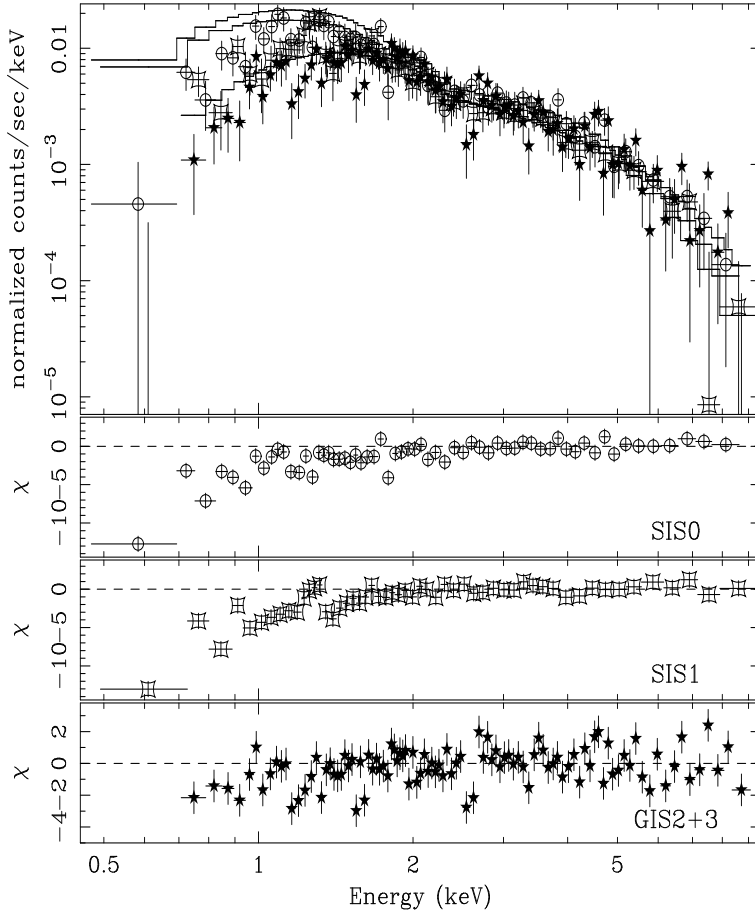


FIG. 1.— **Upper panel:** Joint spectral fit of a power law with fixed Galactic absorption to the SIS0 (circles), SIS1 (squares), and the combined GIS2+GIS3 (stars) data in the restricted 2.5–9.5 keV energy band (with the normalizations untied). The model values (convolved with the detector responses) are represented by lines from upper to lower (at low energies) for SIS0, SIS1, and GIS2+3, respectively. **Lower panel:** Residuals showing deviations of the data from the extrapolation of the fitted model down to the low energy range for all the detectors, respectively.

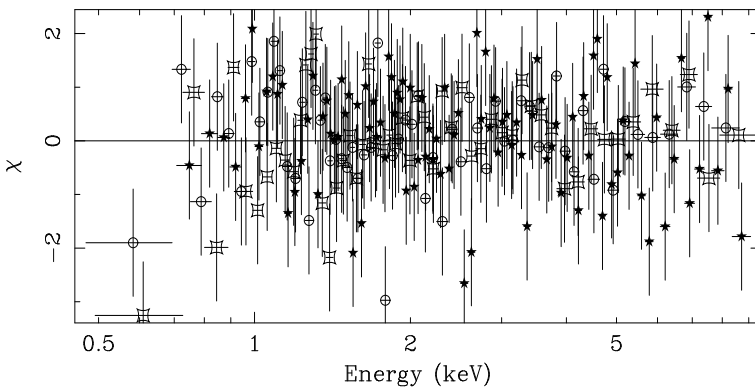


FIG. 2.— Residuals for the best-fit model—a power law with free absorption column density to the joint SIS and GIS data. The SIS data below 0.7 keV are not used in the fitting but plotted for a comparison. The plot symbols are the same as in Fig.1.

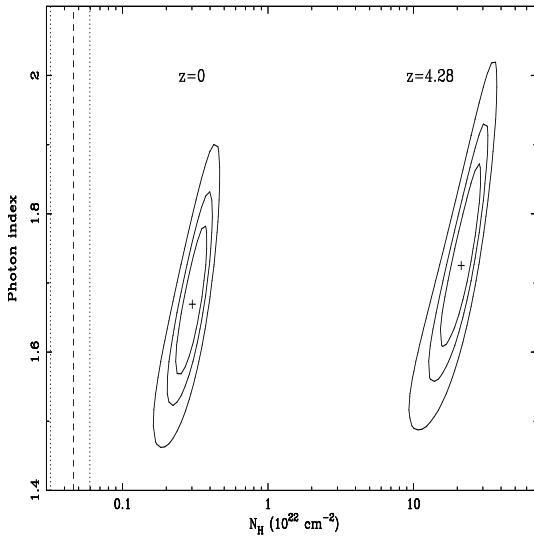


FIG. 3.— Confidence contours of fitted absorption column density and photon index for the total absorption at redshift $z=0$ and for the excess absorption (with additional fixed Galactic absorption) assumed at the quasar redshift $z=4.28$, respectively. The contours are at the 68%, 90%, and 99% confidence, respectively, for two interesting parameters. The elemental abundances are assumed to be the solar values. The best-fit values are indicated by crosses. The Galactic column density and a conservative 30% uncertainty region are indicated by dashed and dotted lines, respectively.

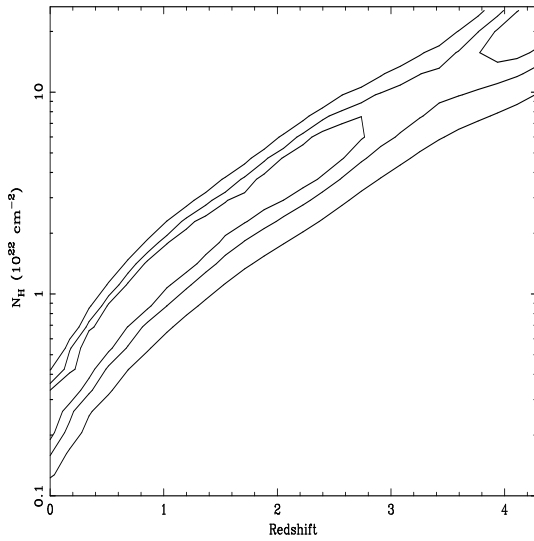


FIG. 4.— Contours of allowed excess absorption $N_{\text{H}}^{\text{exc}}$ and the redshift of the absorber for two interesting parameters at the 68%, 90%, and 99% confidence levels, respectively. The elemental abundances are assumed to be the solar values.

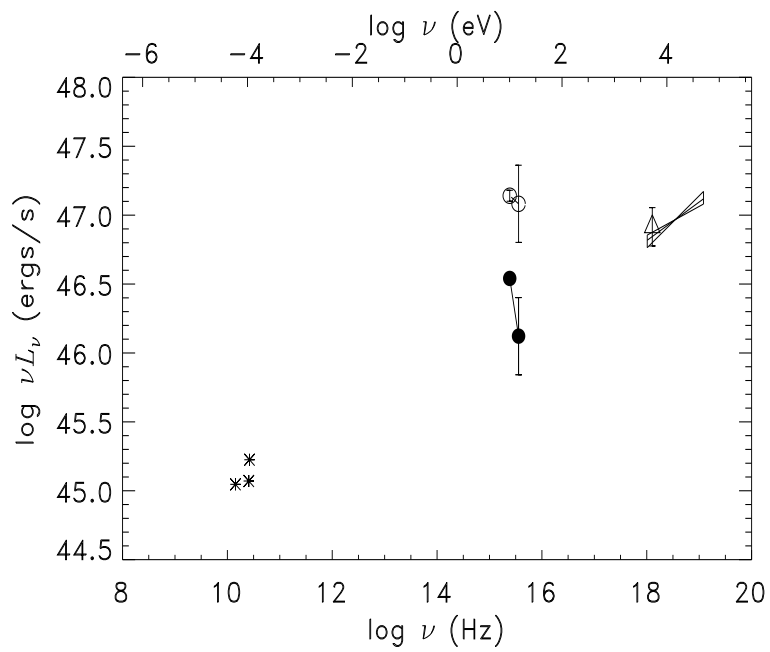


FIG. 5.— Spectral energy distribution of the quasar in the source rest frame, in which the luminosities are at the emitting frequencies. The X-ray luminosities are corrected for the total absorption. The RASS measurement (triangle) is converted from the count rate assuming the spectral model as the extrapolation of the best-fit absorbed power law derived in this work, and at a frequency corresponding to 1 keV in observer frame. The UV luminosities are obtained from the optical B- and R-band (non-simultaneously) photometry data (Zickgraf et al. 1997), with the correction for dust extinction applied for: (a) the Galactic extinction only (filled dots); (b) the Galactic plus an additional column of a local X-ray absorber ($\tau \lesssim 0.1$) assuming the Galactic dust-to-gas ratio (open circles). In the case of the excess absorption occurring at a high redshift or intrinsic to the quasar, the *intrinsic* UV luminosities are uncertain due to the unknown extinction; however, they must be no less than the observed values for which only the correction for the Galactic reddening was applied (filled dots).